Optics and Laser Technology 115 (2019) 97–103

Contents lists available at ScienceDirect

Optics and Laser Technology

journal homepage: www.elsevier.com/locate/optlastec

Full length article

Transition from saturable absorption to reverse saturable absorption of carmoisine dye under low-powered continuous wave laser excitation

M. Abdullah[a,b], H. Bakhtiar[b,c,*], G. Krishnan[b,c], M.S.A. Aziz[b,c], W.H. Danial[d], S. Islam[b,c]

[a] Institute of Nano Optoelectronics Research and Technology (INOR), Universiti Sains Malaysia, 11800 USM, Penang, Malaysia
[b] Laser Center, Ibnu Sina for Scientific and Industrial Research, Universiti Teknologi Malaysia, 81300, Johor Bahru, Johor, Malaysia
[c] Department of Physics, Faculty of Sciences, Universiti Teknologi Malaysia, Johor Bahru, Johor, Malaysia
[d] Department of Chemistry, Kuliyyah of Science, International Islamic University Malaysia, Kuantan, Pahang, Malaysia

HIGHLIGHTS

- FTIR results confirm the occurrence of intermolecular charge transfer (ICT) within the naphtyl-azo bonds.
- SA type of behavior switches to RSA in increasing concentration of carmoisine dye.
- Huge magnitude of $\chi^{(3)}$ was calculated in the order of 10^{-5} esu due to ICT process within the dye molecules.
- Optical limiting (OL) behavior revealed the low OL threshold at 0.01 kW/cm^2.

ARTICLE INFO

Keywords:
Carmoisine
Optical limiter
Optical switching
Z-scan technique
FTIR

ABSTRACT

Unique nonlinear optics (NLO) properties i.e. intensity-dependent nonlinear absorption and refraction of carmoisine (food dye) is studied using a single beam z-scan technique. A switchover behavior from a saturable absorption (SA) to reverse saturable absorption (RSA) is observed by increasing concentration of carmoisine dye. The flip in the absorption response is attributed to the aggregated dye molecules under intense laser beam, which induces the formation of carmoisine dimers. In the UV–Vis absorption analysis, the appearance of two bands at higher concentration confirms the formation of carmoisine dimers. Fourier transform infrared spectroscopy (FTIR) suggests the intermolecular charge transfer (ICT) within the naphtyl-azo bonds. Huge magnitude of $\chi^{(3)}$ is calculated in the order of 10^{-5} esu due to ICT process within the dye molecules. Optical limiting (OL) behavior is observed with low OL action threshold ~0.01 kW/cm^2 under continuous wave laser beam. The experimental findings shows that carmoisine dye has potential as an optical material for photonics applications such as an optical limiter under low-powered continuous wave laser.

1. Introduction

Recently, in modern telecommunication technology, extensive efforts have been devoted towards the nonlinear optical (NLO) behavior of organic materials (dyes) owing to their potential applications in all-optical devices. All-optical devices applications can be achieved via the manipulation of polarization, amplitude, phase/group velocity, and direction of the laser beam passing through a NLO material. That degree of light manipulation can only be achieved by exploiting various NLO phenomena such as saturable absorption (SA), Kerr effect, and reverse saturable absorption (RSA) inside a NLO material [1–3].

Organic dyes have attracted considerable interest especially in 3rd order NLO properties. Organic dyes with delocalized π-conjugated electrons exhibited the high polarizability and fast charge redistribution under intense rapidly-changing electric field i.e. laser beam. In a conjugated molecular system consisting of electrons donating group (D) and electron accepting groups (A), intramolecular charge transfer (ICT) occurred as a result of D-A interactions which leads to stabilization of the system and enhancement of the NLO activities [1]. Extensive studies have been reported on the 3rd order NLO behavior of different dyes such as acid green 25 [1], cationic phenothiazine [4], triphenylmethane [5], azo dyes based on dimedone [6], anthocyanins based dyes [7], betanin-based natural dye [8], red Biebrich scarlet (BS) dye [9], coumarin dyes [10,11], basic blue 55 dye [12], boron dipyrromethene dye [13], Bismarck brown Y dye [14], phthalocyanine-composite materials [15–20], 1,5-diaminoanthraquinone dye [21], brilliant green [22],

* Corresponding author at: Laser Center, Ibnu Sina for Scientific and Industrial Research, Universiti Teknologi Malaysia, 81300, Johor Bahru, Johor, Malaysia.
E-mail address: hazri@utm.my (H. Bakhtiar).

https://doi.org/10.1016/j.optlastec.2019.01.032
Received 4 October 2018; Received in revised form 28 November 2018; Accepted 19 January 2019
Available online 15 February 2019
0030-3992/

basic green 1 [23], natural laccaic acid [24], and azo-dye doped polymer [25]. These dyes often shows prominent NLO response under intense continuous and pulsed laser beam. The detailed comparison of the 3rd order NLO response of these reported organic dyes with the current work are tabulated in Section 3. However, the switchover in the nonlinear absorption behavior from saturable absorption (SA) to reverse saturable absorption (RSA) under low powered CW laser as the concentration of the dye is increased has been scarcely reported in the literature [26]. This unique behavior can be utilized as a new mechanism in the development of all-optical devices. Sreekumar et al. reported the first observation on SA-RSA flipping in increasing concentration of Amido Black dye under low powered He-Ne laser operating at 632.8 nm. The SA-RSA flipping behavior can be explained via the modification in absorbance band due to the aggregation of the dye molecules. This current work reports the interesting switchover from SA to RSA under low-powered continuous wave (CW) laser i.e. at 532 nm excitation wavelength of increasing concentration of carmoisine dye.

Carmoisine (azorubine or E122) is an azo dyes, composed of disodium 4-hydroxy-3-(4-sulfonato-1-naphthylazo) naphthalene-1-sulfonate. The molecules of carmoisine consist of two separate ring systems, the naphthalene (1) ring and naphthalene (2) ring connected to each other by the chromophoric azo group (−N═N−), which has potential as a good NLO material [27]. Moreover, the occurrence of ICT between the naphthalene ring and localized azo bond which extended the π-electron delocalization over the naphtyl-azo system. The intramolecular hyperconjugative interactions between the orbital overlap of π (C−C) and π^* (C−C) bond contributes to the higher hyperpolarizabilities of the carmoisine's molecule which leads to the stabilization of the system [27,28]. According to the author's knowledge, 3rd order optical nonlinearity of the carmoisine dye is rarely reported. This present work deals with the measurement of 3rd order optical nonlinearity of carmoisine dye and its optical limiting performance by the single-beam z-scan technique. The infrared spectroscopy and linear optical properties are also studied to determine its bonding.

2. Materials and methods

2.1. Preparation of carmoisine samples

Commercially available carmoisine solution (5.2% weight percentage) was purchased of StarBrand Company and used without further purification. The chemical structure of the dye is shown in Fig. 1. Deionized water has been used as the solvent for all samples. Series of dilution were performed on the stock carmoisine solution to obtain dye solutions with concentration of 1.33, 3.12, 4.90, 6.69, and 8.47 μM. Fourier transform infrared spectroscopy (FTIR) was performed on the sample using a Perkin Elmer NIR FTIR spectrometer.

2.2. Linear optical response

UV–vis absorbance characterization was performed using Ocean Optics spectrometer setup. The linear absorption coefficient, α at

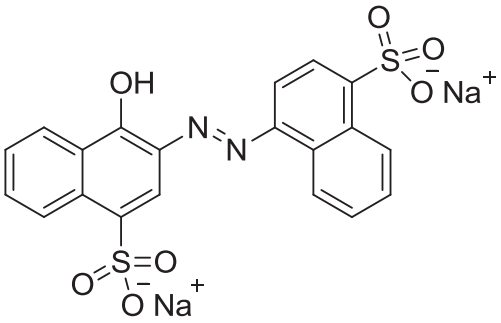

Fig. 1. Chemical structure of Azorubine.

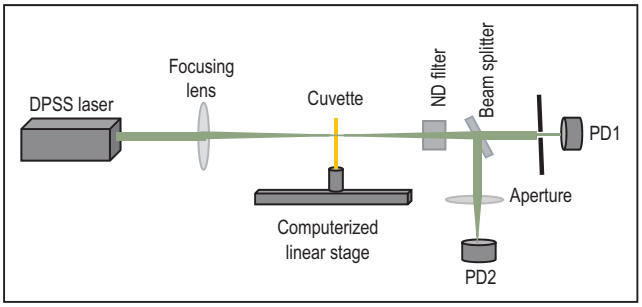

Fig. 2. Z-scan technique.

532 nm was calculated based on the absorbance value. The refractive index, n of the dye samples were measured using a digital refractometer (DR201-95, KRUSS). The value of α and n are listed in Table 2.

2.3. 3rd order NLO characterization

The z-scan setup is schematically shown in Fig. 2. A CW diode pumped solid state (DPSS) laser (Coherent Verdi-V5, 532 nm) was employed as the excitation laser. Two silicon amplified photodetectors (PDA55, Thorlabs) were used in the setup. The dye solution was contained in a quartz cuvette with a path length of 1 mm which was mounted into a precision motorized stage (LTS-300, Thorlabs). The sample path length is much smaller than the Rayleigh length (z_R = 3.1 mm), which is essential prerequisite for z-scan thin sample analysis. During the scan, the dye sample was moved along the z-direction of the laser beam under the control of a computer. A 50:50 beam splitter was used to split the beam into two arms. One of the two photodetectors used was placed after an aperture for the first arm (closed z-scan), while the other was placed in front of a lens for the second arm (open z-scan). Concurrently, the signal from the two photodetectors, were monitored and recorded by an oscilloscope. The phenomena that contribute to nonlinear refraction (NLR) will be studied from closed aperture z-scan, while the open aperture z-scan will be sensitive towards the nonlinear absorption (NLA) response. Table 1 summarizes the parameters of the z-scan setup used in the experiment.

The peak followed by a valley-normalized transmittance obtained from the closed aperture Z-scan is defined as $\Delta T_{P\text{-}V}$ which is given as $T_P - T_v$. The variation of this quantity as a function of $|\Delta\varphi_0|$ is given by $\Delta T_{p-v} = 0.406(1 - S)^{0.25}|\Delta\varphi_0|$, where $|\Delta\varphi_0|$ is the on-axis phase shift at the focus, S is the aperture linear transmittance with r_0 denoting the aperture radius ($S = 1 - \exp(-2r_0^2/\omega_0^2)$, and ω_0 denoting the beam radius at the aperture in the linear regime. Then the intensity-dependent refractive index, n_2 is given by,

$$n_2 = \frac{\Delta\varphi_0\lambda}{2\pi I_0 L_{eff}} \quad (1)$$

where λ is the laser wavelength, I_0 is the intensity of the laser beam at focus $z = 0$, $L_{eff} = \frac{[1-\exp(-\alpha L)]}{\alpha}$, L_{eff} is the effective thickness of the sample, α is the linear absorption coefficient and L is the thickness of the sample.

The nonlinear absorption coefficient, β can be estimated from the

Table 1
Z-scan parameters used.

Parameters	Value
Focal length (f)	20 cm
Aperture radius (r_a)	68 μm
Beam waist (w_0)	23 μm
Wavelength (λ)	532 nm
Aperture linear transmittance (S)	0.23
Rayleigh range (z_R)	0.31 cm

open aperture Z-scan data. The transmittance peak value (DT) of the open aperture curve is related to the β using the relation,

$$\beta = \frac{2\sqrt{2}\Delta T}{I_0 L_{eff}} \tag{2}$$

where ΔT is the one-valley value of open aperture curve. The real and imaginary parts of $\chi^{(3)}$ are evaluated from the n_2 and β coefficients, respectively. The relations are defined as follows:

$$Re\chi^{(3)}\,(\text{esu}) = 10^{-4}\frac{\varepsilon_0 c^2 n_0^2}{\pi} n_2 \left(\frac{\text{cm}^2}{\text{W}}\right) \tag{3}$$

and

$$Im\chi^{(3)}\,(\text{esu}) = 10^{-2}\frac{\varepsilon_0 c^2 n_0^2 \lambda}{4\pi^2}\beta\left(\frac{\text{cm}}{\text{W}}\right) \tag{4}$$

where ε_0 is the vacuum permittivity, and c is the light velocity in vacuum. 2nd order hyper-polarizability, γ describes the interaction of the incident photons with the permanent dipole moment of the dyes. Essentially, it represents the magnitude of $\chi^{(3)}$ response at the molecular level and is related to $\chi^{(3)}$ via equation (5).

$$\gamma = \frac{Im[\chi^{(3)}]}{f^4 C_{mol} N_A} \tag{5}$$

f is the Lorentz field factor and is given by $f = (n^2 + 2)/3$, C_{mol} is the molar concentration, and N_A is the Avogadro constant. The optical limiting response of the samples are assessed from open z-scan arm. The sample was fixed at the focal point, with input power was slowly increased. The transmission against input power was plotted to observe the optical limiting in action.

3. Results and discussions

FTIR spectrum of the carmoisine solution was shown in Fig. 3 in the region 400–4000 cm^{-1}. A good correlation was found between the bands found in our studies with literature [28]. The observed bands and peak were assigned based on literature [27]. The intense broad band peaked at 3441 cm^{-1} is attributed to hydrogen bonded OH stretching vibrations. The in-plane OH deformation vibration also rises strongly at 1502 cm^{-1}. The azo stretching vibration of N=N bond is predicted to occur between 1450 and 1380 cm^{-1} [29]. However, due to greater conjugation and π-electron delocalization, it undergoes a large wavenumber downshift creating a band in 1368 cm^{-1} as in Fig. 3. The stretching mode of C–N group connected to naphthalene ring produces a strong band at 1368 cm^{-1}, whereas the sulfonate (SO^3) group vibration gives the most intense band at 1044 cm^{-1}.

Furthermore, the naphthalene ring vibrations largely contributes to the FTIR spectra. The most important correlation towards NLO properties is within its C=C stretching bands because of it acts as a measurement of the degree of conjugation through the π-electrons chain. ICT from donor to acceptor group though single-double bond conjugated path can greatly enhanced both the molecular dipole moment and molecular polarizability. Since the ICT process contributes to the rises of various C=C stretching bands, therefore C=C stretching modes provides evidence of ICT occurrence through π-system. In our results, C=C stretching modes contributes to several medium and strong bands at 1642, 1605, 1568, 1517 and 1475 cm^{-1} in the spectrum. This confirms the molecule to be highly polarized, hence enhancing the NLO properties. Table 2 summarizes all the vibrational band and its assignment that were present in the FTIR spectra.

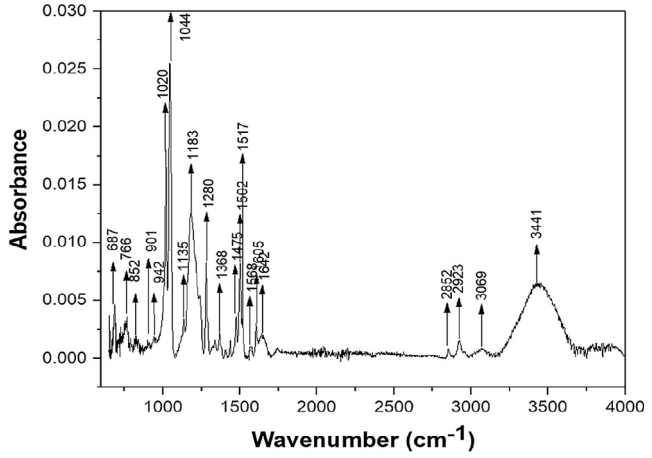

Fig. 3. FTIR spectrum of carmoisine.

Table 2
List of vibrational bands and its assignment. The letter that comes after the wavenumber represent the characteristic of the band (vvs = very very strong, vs = very strong, sh = shoulder, m = medium strong, s = strong, vs = very strong, w = weak, vvw = very very weak).

ν_{IR} (cm^{-1})	Assignments
3441 vs	O–H
3069 sh	C–H
2923 m	Alkyl C–H
2852 m	Alkyl C–H
1642 s	Naph (2) + O–H
1605 s	Naph (1)
1568 m	Naph (2) + O–H
1517 m	Naph (2)
1502 vs	O–H
1475vs	Naph (1)
1437 m	CH Naph (2) + C–N–N
1406 w	CH Naph (1) + Naph (2)
1368 m	N=N + Naph (2)
1338 w	C–H Naph (1, 2) + (C–N N–C)
1280 vs	C–N + CH Naph (2)
1240 vvw	C–O + (C–N N–C)
1211 vvw	C–O + O–H
1183 vvs	C–H Naph (2) + C–N + SO_3
1162 vvw	C–H Naph (1) + C–N
1135 w	C–N + CH Naph (1)
1044 vvs	SO_3 + Naph rings (1,2)
1020 vvs	C–N + CH Naph (1)
942 w	C–N N + Naph rings (1,2)
901 w	Naph rings + C–N N + SO_3
852 w	C–N N + SO_3
816 w	Naph (2) ring + O–H
789 w	Naph (1) ring
766 m	SO_3 + Naph rings
726 w	SO_3 + Naph rings

The UV–VIS absorption spectra of the samples with different concentration were shown in Fig. 4. Several bands were observed in the ultraviolet and visible region. Several bands observed at UV may be ascribed to the excitation of π-electrons which is localized on the naphthyl rings. The visible bands observed between 480 and 580 nm can be attributed to high delocalization of π-electrons in the azo chromophore group that gives the dye its colour. As expected, the linear absorbance monotonously increases with the concentration of the dye solution. Interesting to note that some bands are more apparent at higher dye concentration especially around 400 nm and 540 nm. This can be attributed to the formation of dimers that will be discussed further next. Table 2 shows the linear absorption coefficient, α and refractive index, n at various concentration. α and n represent the linear optical properties of the dye, with both coefficients increase with concentration due to higher amount of solute in the solution.

The open-aperture z-scan curve of carmoisine dye at varying concentration are shown in Fig. 5. When samples were far from the beam waist, minimal nonlinear signals i.e., no change in transmission were observed. Whereas, the abrupt change was observed in the transmission

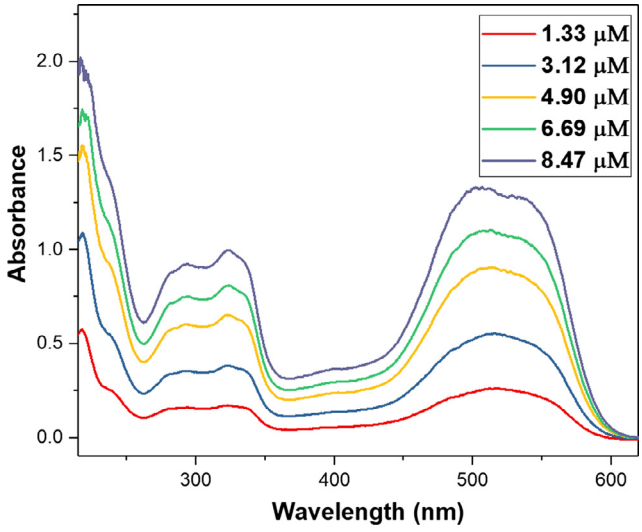

Fig. 4. Absorption spectra of the dye at different concentrations.

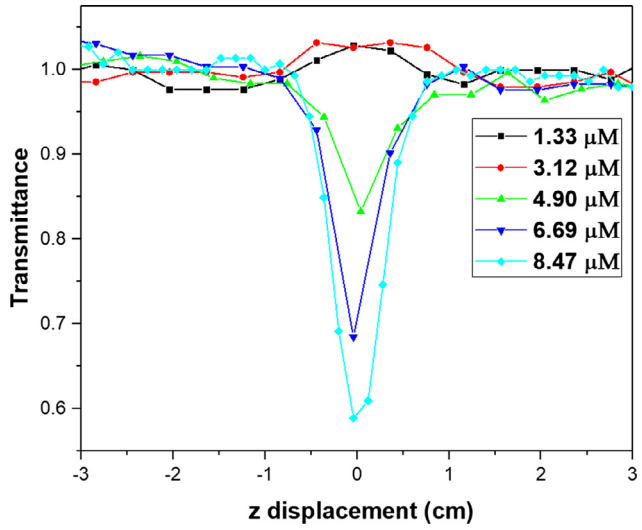

Fig. 5. Open-aperture z-scan of carmoisine at different dye concentrations.

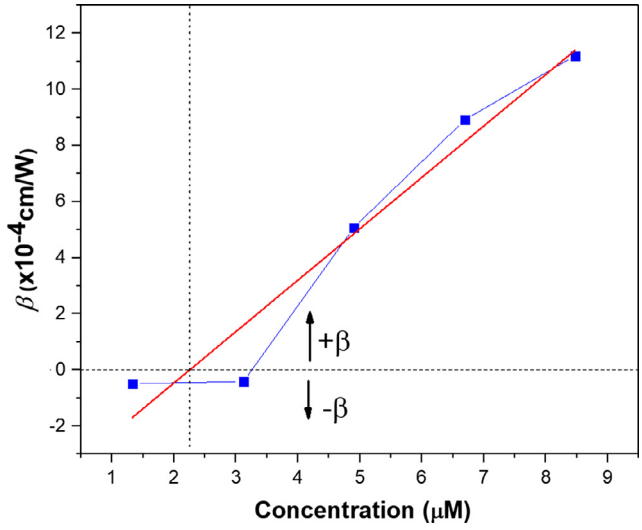

Fig. 6. The value of β of different dye's concentration.

when the sample moved into the nonlinear regime because of the NLA process. Interestingly, transition from saturable absorption (SA) to reverse saturable absorption (RSA) was observed as the concentration increases under 9.3 kW/cm^2 of excitation intensity. This behavior can be attributed to the effect of aggregation on the increase in the dye's concentration. Aggregation in aqueous organic dye solution involves the formation of dimers from monomers [30]. The bonding between monomers creates a new species (dimers) with different absorbance profile, indicated by the rise of the new bands around 400 nm and 540 nm at higher dye concentration (based on Fig. 4). The bonding between dye molecules/monomers also translates into the splitting of the singlet energy states into triplet energy states. Thus, under intense excitation intensity, at lower monomers concentration will lead to SA effect as observed at 1.33 μM and 3.12 μM. Fig. 6 shows the linear relation between the calculated β values with the dye concentration. The negative sign of β represents SA phenomena was dominant on the sample, while positive β suggests that the RSA effect has overcome the SA effect.

Fig. 7 illustrates the mechanism of NLA in the organic dyes. The absorption can occur via several transition processes which are:

(I) from S_0 (ground state) to the S_1 (1st excited state), then T_1 through inter-system crossing (ISC),
(II) from S_0 to S_2,
(III) from S_1 to S_2, and
(IV) from T_1 to T_2.

Generally, transition (II) is said to contribute to two-photon absorption (TPA) phenomena, but if the absorption cross section of excited state is larger than that of ground state, then it is called as the RSA process. Whereas transition (III) and (IV) correspond to excited state absorption (ESA) process. Jeyaram et al., reported that RSA is the major NLA mechanism that occurs in organic dyes [1]. Thus we can infer that ESA assisted RSA is the nonlinear mechanism leading to the observed NLA in higher concentration of carmoisine dye (4.90 μM and above). For the CW excitation, the NLA usually originates from thermo-optics effect, which eventually enhance the ESA process. This explains more prominent RSA effect at higher concentration as more dye molecules are thermally agitated. A further increase in concentration intensifies the RSA process represent by lower transmission at the focal (Fig. 5). The interesting transformation from SA to RSA can be used for optical pulse compressors, optical switching, and laser pulse narrowing. Most importantly, RSA is applied on an optical limiting device that protects sensitive optical components and the human eye, from laser-induced damage.

Fig. 8 represent the closed-aperture z-scan curve of carmoisine at different concentration. To eliminate the role of solvent in the observed results, z-scan measurement was performed for distilled water inside the cuvette; these yielded no nonlinear signals. The peak followed by valley in normalized transmission in Fig. 8 indicated that the dye solutions exhibit self-defocusing effect with negative value of n_2. The self-focusing phenomena can be attributed to thermal in nature, resulting from absorption of laser beam at 532 nm. The localized absorption from the intense laser quickly creates spatial temperature profile across the beam waist. The dependence of temperature towards refractive index means that the phase of the transmitted beam is distorted accordingly. This in turn creates effect which is called thermal lensing. The thermal nature of the NLR was confirmed by measuring the peak to valley separation to be higher than $1.7z_R$ ($6.7z_R$). The quantity $\Delta T_{P\text{-}V}$ were measured for all samples to be used in calculating the value of n_2 from Eq. (2). The values of n_2 calculated were in the order of 10^{-8} cm^2/W (Table 3). Since the nonlinear coefficients of z-scan is very dependent on the pulse width of the laser, comparison with the other types of dye will only be valid for similar laser used during z-scan which is continuous laser. Overall, the value of n_2 calculated is within the range of other reported azo dyes [6121426].

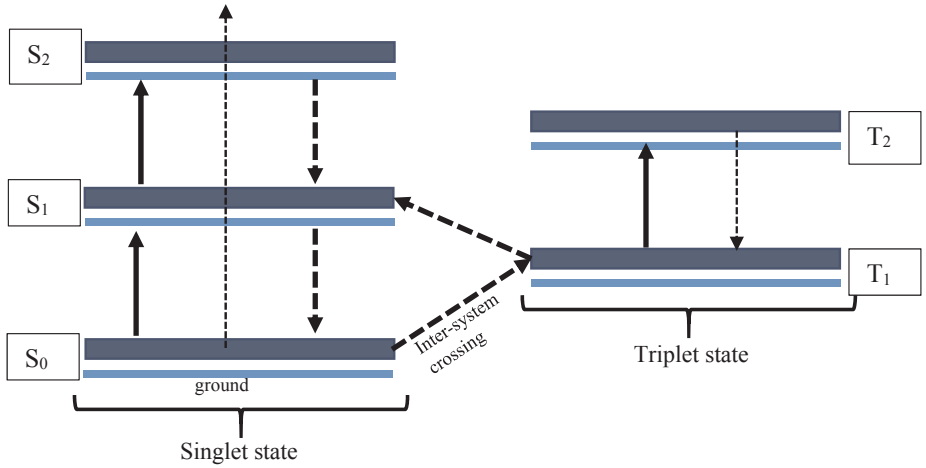

Fig. 7. Illustration of typical 5 energy level model of an organic dye. Straight line with arrow represent radiative transition and non-radiative transitions by dotted lines.

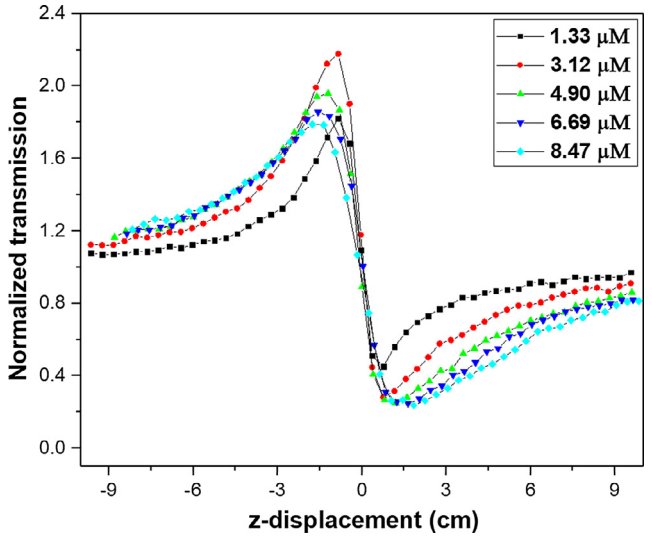

Fig. 8. Closed aperture z-scan of carmoisine at varying concentrations.

Table 3
α and n coefficient at different concentration.

Concentration (μM)	α (cm^{-1})	n
1.33	−0.55963	1.3325
3.12	−1.19986	1.3330
4.90	−1.98519	1.3331
6.69	−2.4573	1.3332
8.47	−2.92942	1.3332

Unlike that in NLA, the NLR does not shows significant change towards different concentrations under the same focal intensity of 5.5 kW/cm^2. The peak transmittance were in the range of 1.8–2.2, whereas the valley at around 0.25–0.4. This is supported the value of n_2 which in the range 4.6×10^{-8} to 7.36×10^{-8} cm^2/W in Table 4. This trend in Fig. 9 may be attributed to the presence of prominent ESA that has been discussed before. At the lowest concentration (1.33 μM), contribution of ESA is suppressed due to small number of molecules involved within the beam waist of the laser. Furthermore, the electronic origin that contribute to NLR would be lowest at this condition. At the concentration of 3.13 μM, the absorption-turn thermalization process results in overwhelming thermal lensing effect, thus higher n_2 value which can be seen from Fig. 9. However further increase in concentration (3.12 μM and higher), the redistribution of population during ESA might further reduce the transmittance, which subsequently weaken the nonlinear refractivity of the material.

Table 4 shows the value of n_2, β, real and imaginary parts of $\chi^{(3)}$, the magnitude of $\chi^{(3)}$, $|\chi^{(3)}|$, and hyper-polarizability, γ. It is known that *Re* $\chi^{(3)}$ and *Im* $\chi^{(3)}$ depends upon n_2 and β respectively. Here, the value of *Re* $\chi^{(3)}$ is higher for low concentration indicating the dominance of NLR, whereas the at higher concentration (above 4.9 μM) the *Im* $\chi^{(3)}$ surpasses the *Re* $\chi^{(3)}$ suggesting the prominence of NLA.

The materials with RSA property are widely used for optical limiting (OL) applications. Fig. 10(a) shows the input intensity vs output signals recorded from open z-scan setup. At low input power, the sample show a linear response of output power, obeying Beer-Lambert's law. As the input power increases, the output power deviates from linearity and OL action with saturated output power was observed at higher intensity. The OL threshold represents the intensity at which the optical limiting action starts to take place. From the graph of normalized transmission against input intensity. The OL performance is represents by its limiting threshold intensity, measured at 50% of the transmittance from Fig. 10(b) (value in Table 5). As expected, the limiting threshold increases monotonously with dye's concentration. However, huge improvement in OL threshold was observed at 8.47 μM due to the formation of dimers and huge value of $|\chi^{(3)}|$.

4. Conclusions

Different concentration of aqueous carmoisine dye solutions have been prepared. FTIR analysis shows confirms the ICT process within the naphtyl-azo bonds. UV–VIS analysis shows the absorption bands around 280 nm, 320 nm, and 520 nm, which the latter is in the vicinity of the excitation wavelength used in the z-scan technique. Open z-scan characterization reveals a flip from SA to RSA with the increase in the concentration which can be explained due to formation of dimers. Stronger RSA effect was observed at higher concentration which is represented by the linear relationship between β and the dye's concentration. Closed z-scan curve shows that the dye exhibited self-defocusing effect with negative value of n_2. Both self-focusing effect and strong RSA behavior of the dye contributes to low-threshold optical limiting action at 0.01 kW/cm^2. The experimental findings shows the possibility of utilizing this low-threshold NLO material as a smart material for potential applications as an optical limiter.

Acknowledgement

The authors would like to thank the Malaysia Ministry of Education and Universiti Teknologi Malaysia for their financial support through

Table 4
The estimated values of 3rd order NLO coefficients of carmoisine dye solutions at various concentration, along with some of the recently reported values under low powered CW laser excitation.

NLO material	Concentration (μM)	n_2 ($\times 10^{-8}$ cm^2/W)	$Re\ \chi^{(3)}$ ($\times 10^{-5}$ esu)	β ($\times 10^{-4}$ cm/W)	$Im\ \chi^{(3)}$ ($\times 10^{-5}$ esu)	$\lvert\chi^{(3)}\rvert$ ($\times 10^{-5}$ esu)	γ ($\times 10^{-19}$ esu)
Carmoisine dye at 532 nm laser excitation	1.33	−4.723	−0.2127	−0.4898	−0.0968	0.2337	0.4820
	3.12	−7.257	−0.3270	−0.4110	−0.0812	0.3370	0.1723
	4.90	−7.087	−0.3194	5.0701	1.0017	1.0514	1.3505
	6.69	−6.667	−0.3005	8.9128	1.7609	1.7864	1.7396
	8.47	−6.323	−0.2850	11.1968	2.2122	2.2305	1.7248
Amido black dye-PVA film at 632.8 nm laser excitation [26]	129.8	−16.6	–	−16	–	0.206	–
	389.0	−17.7	–	−34.7	–	0.309	–
	1622.0	−41.1	–	17.6	–	0.522	–
1,4-Diamino-9,10-Anthraquionone dye at 532 nm excitation [31]	4	103.61	4.9007	2.1	0.00042	4.9	–
	6	127.00	6.0426	3.0	0.00060	6.0	–
	8	146.71	6.9942	3.7	0.00074	7.0	–
	15	183.62	8.7547	4.4	0.00092	8.8	–
	21	201.50	9.5636	5.5	0.00111	9.6	–
Betanin natural dye-ZnO at 473 nm laser excitation [8]	300	98.5	0.125	122.1	0.584	0.597	–

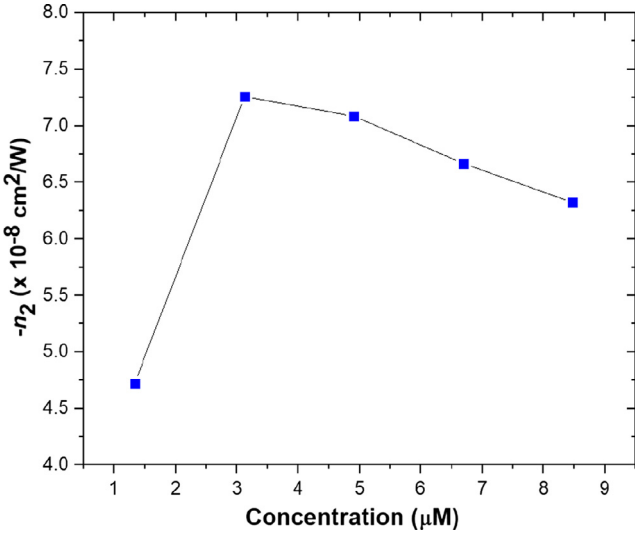

Fig. 9. The effect of concentration of dye towards the value of n_2.

Table 5
Limiting threshold of carmoisine dye at different concentration.

Concentration (μM)	Limiting threshold (kW/cm^2)
1.33	0.0626
3.12	0.0287
4.90	0.0203
6.69	0.0166
8.47	0.0115

Tier 1 with vote 18H67. Special thanks also to Universiti Teknologi Malaysia for the postdoctoral scheme under vote number 04E08 for Mundzir Abdullah. Corresponding author is grateful to the Malaysia Ministry of Education through the FRGS fund with vote 03EE89.

Appendix A. Supplementary material

Supplementary data to this article can be found online at https://doi.org/10.1016/j.optlastec.2019.01.032.

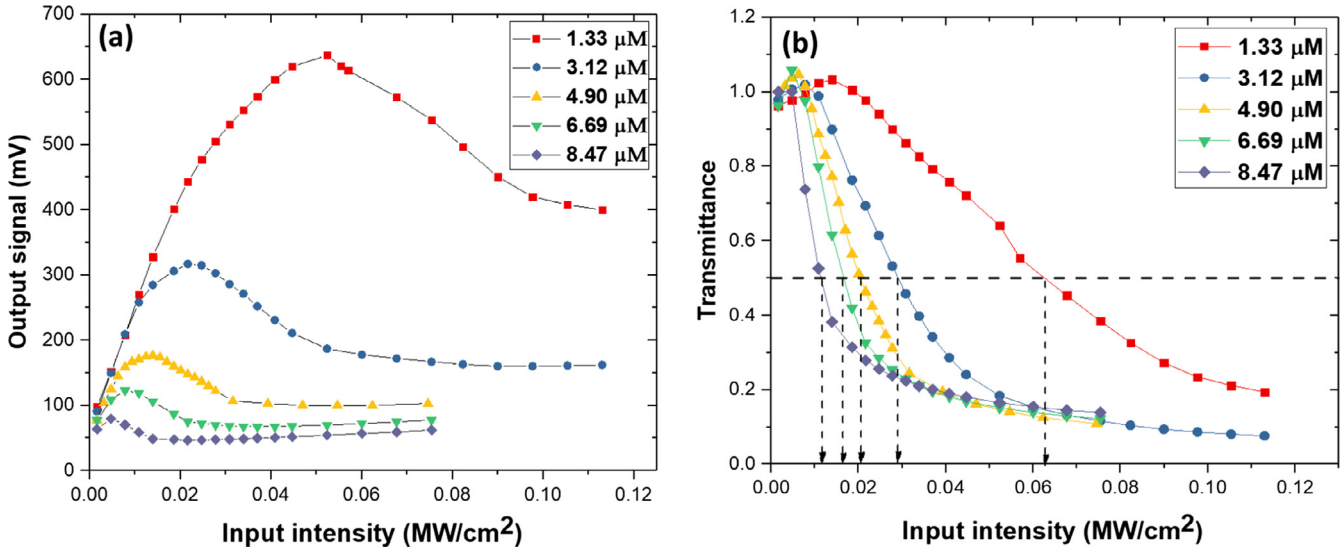

Fig. 10. (a) The output signal taken during the optical limiting measurement. (b) The transmittance vs the input in Optical limiting performance of the carmoisine dye at different concentrations.

References

[1] S. Jeyaram, T. Geethakrishnan, Third-order nonlinear optical properties of acid green 25 dye by Z–scan method, Opt. Laser Technol. 89 (2017) 179–185, https://doi.org/10.1016/j.optlastec.2016.10.006.

[2] S.R. Marder, Organic nonlinear optical materials: where we have been and where we are going, Chem. Commun. (2006) 131–134, https://doi.org/10.1039/b512646k.

[3] M.G.P.S. Fernando, K.A.I.L. Wijewardena Gamalath, Modelling all-optical switching and limiting properties of AlAs photonic crystals, Int. Lett. Chem. Phys. Astron. 77 (2018) 1–14, https://doi.org/10.18052/www.scipress.com/ILCPA.77.1.

[4] V. Viswanath, C.I. Muneera, Nonlinear Refraction behaviour of toluidine blue O dye-PVA nanocomposite films under CW laser light excitation, Opt. Laser Technol. 4 (2017) 1, https://doi.org/10.1016/j.matpr.2017.04.013.

[5] T. Geethakrishnan, P.K. Palanisamy, Z-scan determination of the third-order optical nonlinearity of a triphenylmethane dye using 633 nm He-Ne laser, Opt. Commun. 270 (2007) 424–428, https://doi.org/10.1016/j.optcom.2006.09.035.

[6] H. Motiei, A. Jafari, R. Naderali, Third-order nonlinear optical properties of organic azo dyes by using strength of nonlinearity parameter and Z-scan technique, Opt. Laser Technol. 88 (2017) 68–74, https://doi.org/10.1016/j.optlastec.2016.09.011.

[7] Y. El Kouari, A. Migalska-Zalas, A.K. Arof, B. Sahraoui, Computations of absorption spectra and nonlinear optical properties of molecules based on anthocyanidin structure, Opt. Quant. Electron. 47 (2015) 1091–1099, https://doi.org/10.1007/s11082-014-9965-4.

[8] A. Thankappan, S. Thomas, V.P.N. Nampoori, Effect of betanin natural dye extracted from red beet root on the non linear optical properties ZnO nanoplates embedded in polymeric matrices, J. Appl. Phys. 112 (2012) 1–6, https://doi.org/10.1063/1.4768930.

[9] F. Nasseri, E. Rokhsat, D. Dorranian, Low power continues wave nonlinear optics in red BS dye doped PVA thin film, Optik (Stuttg) 127 (2016) 6813–6820, https://doi.org/10.1016/j.ijleo.2016.05.026.

[10] B. Anand, N. Roy, S. Siva Sankara Sai, R. Philip, Spectral dispersion of ultrafast optical limiting in Coumarin-120 by white-light continuum Z-scan, Appl. Phys. Lett. 102 (2013) 1–5, https://doi.org/10.1063/1.4807151.

[11] K.N. Sharafudeen, A. Adithya, S. Vijayakumar, P. Sudheesh, B. Kalluraya, K. Chandrasekharan, Multiphoton absorption process and self-focusing effect in coumarin derivative doped PMMA films by z-scan and optical limiting studies, Curr. Appl. Phys. 11 (2011) 1089–1093, https://doi.org/10.1016/j.cap.2011.02.001.

[12] M.K. Sadigh, M.S.S. Zakerhamidi, M. Khadem Sadigh, M.S.S. Zakerhamidi, Third order nonlinear responses of Basic Blue 55 molecules in polar solvents, Optik (Stuttg) 130 (2017) 743–749, https://doi.org/10.1016/j.ijleo.2016.10.134.

[13] G. Kubheka, K. Sanusi, J. Mack, T. Nyokong, Optical limiting properties of 3,5-dipyrenylvinyleneBODIPY dyes at 532 nm, Spectrochim. Acta – Part A Mol. Biomol. Spectrosc. 191 (2018) 357–364, https://doi.org/10.1016/j.saa.2017.10.021.

[14] K.A. Al-adel, H.A. Badran, x (3) measurements and optical limiting in Bismarck Brown Y dye, Int. J. Emerg. Technol. Comput. Appl. Sci. International Association of Scientific Innovation and Research (IASIR), 2014, pp. 64–68.

[15] X. Zhao, X.Q. Yan, Q. Ma, J. Yao, X.L. Zhang, Z.B. Liu, J.G. Tian, Nonlinear optical and optical limiting properties of graphene hybrids covalently functionalized by phthalocyanine, Chem. Phys. Lett. 577 (2013) 62–67, https://doi.org/10.1016/j.cplett.2013.04.023.

[16] N. Nwaji, B. Jones, J. Mack, D.O. Oluwole, T. Nyokong, Nonlinear optical dynamics of benzothiazole derivatized phthalocyanines in solution, thin films and when conjugated to nanoparticles, J. Photochem. Photobiol. A Chem. 346 (2017) 46–59, https://doi.org/10.1016/j.jphotochem.2017.05.042.

[17] A. Fashina, T. Nyokong, Nonlinear optical response of tetra and mono substituted zinc phthalocyanine complexes, J. Lumin. 167 (2015) 71–79, https://doi.org/10.1016/j.jlumin.2015.06.003.

[18] O.M. Bankole, T. Nyokong, Nonlinear optical response of a low symmetry phthalocyanine in the presence of gold nanoparticles when in solution or embedded in poly acrylic acid polymer thin films, J. Photochem. Photobiol. A Chem. 319–320 (2016) 8–17, https://doi.org/10.1016/j.jphotochem.2015.12.014.

[19] R.S.S. Kumar, S.V. Rao, L. Giribabu, D.N. Rao, Femtosecond and nanosecond nonlinear optical properties of alkyl phthalocyanines studied using Z-scan technique, Chem. Phys. Lett. 447 (2007) 274–278, https://doi.org/10.1016/j.cplett.2007.09.028.

[20] S.V. Rao, N. Venkatram, L. Giribabu, D.N. Rao, Ultrafast nonlinear optical properties of alkyl-phthalocyanine nanoparticles investigated using Z-scan technique, J. Appl. Phys. 105 (2009) 2–7, https://doi.org/10.1063/1.3079801.

[21] M.C. Sreenath, I. Hubert Joe, V.K. Rastogi, Third-order optical nonlinearities of 1,5-Diaminoanthraquinone for optical limiting application, Opt. Laser Technol. 108 (2018) 218–234, https://doi.org/10.1016/j.optlastec.2018.06.056.

[22] R.K. Choubey, S. Medhekar, R. Kumar, S. Mukherjee, S. Kumar, Study of nonlinear optical properties of organic dye by Z-scan technique using He-Ne laser, J. Mater. Sci. Mater. Electron. 25 (2014) 1410–1415, https://doi.org/10.1007/s10854-014-1743-3.

[23] Q.M. Ali, P.K. Palanisamy, Investigation of nonlinear optical properties of organic dye by Z-scan technique using He-Ne laser, Optik (Stuttg) 116 (2005) 515–520, https://doi.org/10.1016/j.ijleo.2005.05.001.

[24] S. Zongo, K. Sanusi, J. Britton, P. Mthunzi, T. Nyokong, M. Maaza, B. Sahraoui, Nonlinear optical properties of natural laccaic acid dye studied using Z-scan technique, Opt. Mater. (Amst) 46 (2015) 270–275, https://doi.org/10.1016/j.optmat.2015.04.031.

[25] T. He, Y. Cheng, Y. Du, Y. Mo, Z-scan determination of third-order nonlinear optical nonlinearity of three azobenzenes doped polymer films, Opt. Commun. 275 (2007) 240–244, https://doi.org/10.1016/j.optcom.2007.03.018.

[26] G. Sreekumar, P.G.L. Frobel, C.I. Muneera, K. Sathiyamoorthy, C. Vijayan, C. Mukherjee, Saturable and reverse saturable absorption and nonlinear refraction in nanoclustered Amido Black dye-polymer films under low power continuous wave He-Ne laser light excitation, J. Opt. A: Pure Appl. Opt. 11 (2009), https://doi.org/10.1088/1464-4258/11/12/125204.

[27] M. Snehalatha, C. Ravikumar, I. Hubert Joe, N. Sekar, V.S. Jayakumar, Spectroscopic analysis and DFT calculations of a food additive Carmoisine, Spectrochim. Acta – Part A Mol. Biomol. Spectrosc. 72 (2009) 654–662, https://doi.org/10.1016/j.saa.2008.11.017.

[28] M.S.C. Ravikumar, N.S.V.S. Jayakumar, I.H. Joe, Vibrational spectral studies and ab initio computations of a nonlinear food dye carmoisine, Perspect. Vib. Spectrosc. ICOPVS 2008, 2008, pp. 98–101.

[29] L.J. Bellamy, The Infra-red Spectra of Complex Molecules, first ed., Springer, Netherlands, 1975.

[30] F.P. Schäfer, W. Schmidt, J. Volze, Organic dye solution laser, Appl. Phys. Lett. (1966), https://doi.org/10.1063/1.1754762.

[31] S. Zafar, Z.H. Khan, M. Khan, Experimental and theoretical investigations of nonlinear optical properties of 1,4-diamino-9,10-anthraquionone, Spectrochim. Acta – Part A Mol. Biomol. Spectrosc. 114 (2013) 164–169, https://doi.org/10.1016/j.saa.2013.05.001.